PCCP

RSC Publishing

PAPER

View Article Online
View Journal | View Issue

Electrophoresis of a soft sphere in a necked cylindrical nanopore

Cite this: *Phys. Chem. Chem. Phys.*, 2013, **15**, 11758

Shiojenn Tseng,[a] Jyh-Ping Hsu,*[b] Hong-Ming Lo[c] and Li-Hsien Yeh*[d]

Received 25th March 2013,
Accepted 13th May 2013

DOI: 10.1039/c3cp51254a

www.rsc.org/pccp

The influence of boundary shape on electrophoresis is modeled by considering a soft spherical particle comprising a positively charged rigid core and an uncharged membrane layer on the axis of a necked cylindrical pore with its throat positively charged. The presence of the throat makes the associated flow and electric fields nonuniform, yielding several interesting behaviors. In general, the reduction in the cross-section area of the pore intensifies the local electric field and, therefore, accelerates the particle. It also makes the ionic distribution nonuniform, and the electric field induced accelerates the particle. The maximum mobility occurs at the center of a throat, and the higher the charge density of the throat the larger the ratio of maximum mobility/mobility far away from the throat. This result is informative for the design of separation devices having variable cross sectional area.

1. Introduction

With recent developments in lab-on-a-chip and nanofluidic devices for bioanalytical, biomedical, and environmental applications, the transport of colloidal particles, including biocolloids such as cells, proteins, and DNAs, in microfluidics/nanofluidics has received considerable attention.[1–9] In particular, electrophoresis has been widely used both as an analytical tool to characterize the surface properties of an entity and a method to separate and manipulate entities of varying nature. Numerous efforts have been made towards the electrophoresis analysis of entities in an unbounded medium[10–14] and a bounded one.[15–23] In the latter, a cylindrical channel[16–22] was often adopted to study the boundary effect on electrophoresis.

With recent advances in fabrication techniques, microchannels and nanotubes with non-uniform cross sectional areas have emerged as a novel platform for achieving superfast electrophoresis,[24] characterizing zeta potential of nanoparticles,[25] sizing and separating biological entities,[8,26–32] and stretching individual DNA molecules for genomic analysis.[33–35] In contrast to the electrokinetic particle transport through channels with uniform cross sectional area (*e.g.*, cylindrical channels), where the electric field is almost uniform, the electric field varies significantly in a channel with varying cross sectional area. The non-uniform electric field, in turn, affects both the electric and the hydrodynamic forces exerted on a particle, making its electrophoretic behavior in the channel different from that in a channel having uniform cross sectional area. It was found that the electrophoresis of a rigid sphere in a converging–diverging nanotube[29] and in a microchannel[30] can be significantly accelerated as it traverses the converging–diverging section. This phenomenon was also observed experimentally by Xuan *et al.*,[31] where the electrokinetic transport of polystyrene particles through a converging–diverging microchannel was analyzed, and was attributed to an intensification of the local electric field in the converging–diverging section. Recently, Ai *et al.*[32] demonstrated that, due to a strong negative dielectrophoretic force arising from the interaction between a dielectric particle and a spatially non-uniform electric field, the particle can be chocked near the throat of a converging–diverging microchannel.

Previous theoretical analyses on the electrokinetic particle transport through a converging–diverging channel focused mainly on rigid entities. However, most of the biological entities, such as cells, proteins, and DNAs, examined in microfluidics and nanofluidics are non-rigid or soft, that is, their surfaces are penetrable to ions and fluid, implying that extending the analyses for rigid entities to non-rigid ones is necessary. Several efforts have been made towards the electrophoresis of soft particles,[36–44] which comprise a rigid core and an ion-penetrable membrane layer. It was found that, in general, the electrophoretic behavior of a soft particle can be different both qualitatively and quantitatively from that of a rigid one.

In this study, the electrophoresis of a soft spherical particle comprising a positively charged rigid core and an uncharged

[a] *Department of Mathematics, Tamkang University, Tamsui, Taipei, Taiwan 25137*
[b] *Department of Chemical Engineering, National Taiwan University, Taipei, Taiwan 10617. E-mail: jphsu@ntu.edu.tw; Fax: +886-2-23623040; Tel: +886-2-23637448*
[c] *Institute of Polymer Science and Engineering, National Taiwan University, Taipei, Taiwan 10617*
[d] *Department of Chemical and Materials Engineering, National Yunlin University of Science and Technology, Yunlin, Taiwan 64002. E-mail: lhyeh@yuntech.edu.tw*

membrane layer along the axis of a necked cylindrical nanopore with its throat positively charged is theoretically analyzed for the first time. This takes account of both the nature of a particle and that of a boundary shape. Note that because the throat of the nanopore is charged, the associated electroosmotic flow (EOF), which is capable of significantly influencing the behavior of a particle, needs to be considered. The key parameters, including the softness of the membrane layer of a particle, the electric double layer (EDL) thickness, the throat length of the pore, and the surface charge density of the rigid core of the particle and that of the throat, are examined in detail for their influences on the electrophoretic mobility of the particle through numerical simulation.

2. Theory

Referring to Fig. 1, we consider the electrophoresis of a soft spherical particle composed of a rigid core of radius a and a membrane layer of thickness c along the axis of a long cylindrical pore subject to an applied electric field $\boldsymbol{E}$ of strength E. The pore is divided into four sections, a throat section of length l, a converging section and a diverging section, both of width w and height h, and a straight section of radius b. Let d be the distance between the center of the throat and that of the particle. r and z are the radial and the axial distances of the cylindrical coordinates chosen with their origin at the center of the particle. $\boldsymbol{E}$ is in the z direction. Furthermore, we assumed that the applied electric field is relatively low compared to that established by the particle and/or the boundary. Let Ω_a, Ω_b, Ω_c, Ω_d, Ω_m, Ω_n, Ω_i and Ω_o be the surfaces of the particle, the straight section, the converging section, the diverging section, the membrane layer–fluid interface, the neck, the inlet and the outlet of the pore, respectively. The pore is filled with an incompressible aqueous Newtonian fluid containing z_1:z_2 electrolytes, z_1 and z_2 being respectively the valences of cations and anions, with $\alpha = -z_2/z_1$. To focus on the influence of the boundary shape on the electrophoresis of a soft particle, the possible presence of the ion concentration polarization[45–47] arising from the selective transport of ions in the nanopore is neglected.

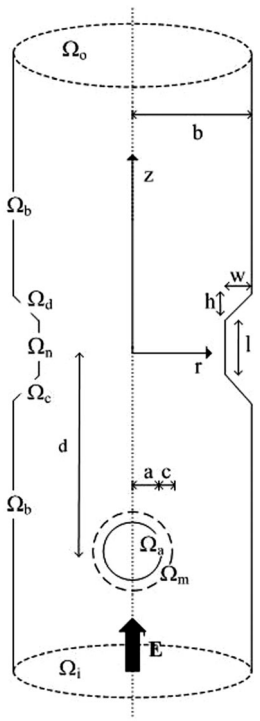

Fig. 1 Electrophoresis of a soft sphere comparing a rigid core of radius a and a membrane layer of thickness c along the axis of a long cylindrical pore subject to an applied electric field $\boldsymbol{E}$ in the z direction; the pore has four sections, a throat section of length l, a converging and a diverging sections of width w and height h, and a straight section of radius b; d is the distance between the center of the throat and that of the particle; r and z are the radial and axial distances of the cylindrical coordinates adopted with the origin at the center of the pore; Ω_a, Ω_b, Ω_c, Ω_d, Ω_n, Ω_m, Ω_i, and Ω_o are the surfaces of the particle, the straight section, the converging section, the diverging section, the neck, the membrane layer–fluid interface, the inlet, and the outlet of the pore, respectively.

Under a pseudo steady-state condition, the present problem can be described by

$$\nabla^2\phi = -\frac{\rho + i\rho_{\mathrm{fix}}}{\varepsilon} = -\sum_{j=1}^{2}\frac{z_j e n_j}{\varepsilon} - i\frac{\rho_{\mathrm{fix}}}{\varepsilon} \quad (1)$$

$$\nabla\cdot\boldsymbol{u} = 0 \quad (2)$$

$$-\nabla p + \eta\nabla^2\boldsymbol{u} - \rho\nabla\phi - i\gamma\boldsymbol{u} = \boldsymbol{0} \quad (3)$$

$$\nabla\left[-D_j\left(\nabla n_j + \frac{z_j e}{k_{\mathrm{B}}T}n_j\nabla\phi\right) + n_j\boldsymbol{u}\right] = 0 \quad (4)$$

Here, ∇ and ∇^2 are the gradient and the Laplace operators, respectively, ϕ, ε, ρ, ρ_{fix}, e, k_{B}, and T are the electrical potential, the permittivity of the liquid phase, the space charge density of mobile ions, the fixed charge density in the membrane layer, the elementary charge, the Boltzmann constant, and the absolute temperature, respectively. D_j, n_j, and z_j are the diffusion coefficient, the number concentration, and the valence of ionic species j, respectively. $\boldsymbol{u}$, η, γ, and p are the velocity, the viscosity, the hydrodynamic frictional coefficient of the membrane layer per unit volume, and the pressure of the liquid phase, respectively; i is a region index: i is 1 or 0 for the membrane layer and the liquid phase outside it, respectively.

We assume that $\boldsymbol{E}$ is much weaker than the electric field established by the particle and the pore, and therefore, $\boldsymbol{u}$, p, ϕ, n_j, and ρ are partitioned into an equilibrium component and a perturbed component, denoted, respectively, by subscript e and prefix δ, respectively, as $\boldsymbol{u} = \boldsymbol{u}_e + \delta\boldsymbol{u}$, $p = p_e + \delta p$, $\phi = \phi_e + \delta\phi$, $n_j = n_{je} + \delta n_j$, and $\rho = \rho_e + \delta\rho$.[10,36,48] The equilibrium (perturbed) component of a variable is obtained from its value in the absence (presence) of $\boldsymbol{E}$.

We consider the case where both the double layer thickness and the level of ϕ can be arbitrary, implying that the effect of double-layer polarization (DLP) might be significant. To model this effect, n_j is expressed as[20,48]

$$n_j = n_{j0}\exp\left[-\frac{z_j e(\phi_e + \delta\phi + g_j)}{k_{\mathrm{B}}T}\right],\ j = 1, 2, \quad (5)$$

where g_j is a hypothetical potential with n_{j0} being the bulk ionic concentration of ionic species j.

It can be shown that, under the condition of weak $\boldsymbol{E}$, eqn (1)–(4) yield the scaled equations:[20,49,50]

$$\nabla^{*2}\phi_e^* = -\frac{(\kappa a)^2}{(1+\alpha)}\left[\exp(-\phi_e^*) - \exp(\alpha\phi_e^*)\right] - iQ^* \tag{6}$$

$$\nabla^{*2}\delta\phi^* = \frac{(\kappa a)^2}{(1+\alpha)}\left[(\delta\phi^* + g_1^*)\exp(-\phi_e^*) + \alpha(\delta\phi^* + g_2^*)\exp(\alpha\phi_e^*)\right]\delta\phi^* \tag{7}$$

$$\nabla^{*2}g_1^* - \nabla^*\phi_e^*\cdot\nabla^* g_1^* = \mathrm{Pe}_1\boldsymbol{u}^*\cdot\nabla^*\phi_e^* \tag{8}$$

$$\nabla^{*2}g_2^* + \alpha\nabla^*\phi_e^*\cdot\nabla^* g_2^* = \mathrm{Pe}_2\boldsymbol{u}^*\cdot\nabla^*\phi_e^* \tag{9}$$

$$-\nabla^*\delta p^* + \nabla^{*2}\boldsymbol{u}^* + (\nabla^{*2}\phi_e^* + iQ^*)\nabla^*\delta\phi^* + \nabla^{*2}\delta\phi^*\nabla^*\phi_e^* = i(\lambda a)^2\boldsymbol{u}^* \tag{10}$$

$$\nabla^\star\cdot\boldsymbol{u}^\star = 0 \tag{11}$$

$$n_1^* = \exp(-\phi_e^*)[1 - (\delta\phi^* + g_1^*)] \tag{12}$$

$$n_2^* = \exp(\alpha\phi_e^*)[1 + \alpha(\delta\phi^* + g_2^*)] \tag{13}$$

Here, $\nabla^\star = a\nabla^*$ and $\nabla^{\star 2} = a^2\nabla^{*2}$ are the scaled gradient operator and the scaled Laplace operator, respectively; $\kappa = \left[\sum_{j=1}^{2} n_{j0}(ez_j)^2/\varepsilon k_B T\right]^{1/2}$ is the reciprocal Debye length; $n_j^* = n_j/n_{j0}$, $\phi_e^* = \phi_e/\zeta_a$, $\delta\phi^\star = \delta\phi/\zeta_a$, $Q^\star = \rho_{\mathrm{fix}}/(\varepsilon\zeta_a/a^2)$, and $g_j^* = g_j/\zeta_a$ with $\zeta_a = k_B T/z_1 e$ being the thermal potential; $\mathrm{Pe}_j = \varepsilon{\zeta_a}^2/\eta D_j$ is the electric Peclet number of ionic species j, j = 1, 2; $\boldsymbol{u}^\star = \boldsymbol{u}/U_{\mathrm{ref}}$ and $\delta p^\star = \delta p/p_{\mathrm{ref}}$ with $U_{\mathrm{ref}} = \varepsilon{\zeta_a}^2/\eta a$ and $p_{\mathrm{ref}} = \varepsilon{\zeta_a}^2/a^2$ being a reference velocity and a reference pressure, respectively; $\lambda^{-1} = (\eta/\gamma)^{1/2}$ is the softness parameter of the particle's membrane layer,[51] which also denotes a shielding length characterizing the extent of flow penetration into that layer.[52] Because the particle is stagnant at equilibrium, $\boldsymbol{u}_e = 0$, and therefore, $\boldsymbol{u} = \delta\boldsymbol{u}$.

Suppose that both the rigid core of the particle and the pore are non-conductive, ion-impermeable, non-slip, and remained at a constant surface charge density. Then the following boundary conditions apply:

$$\boldsymbol{n}\cdot\nabla\phi_e^* = -\sigma_a^* \text{ on } \Omega_a \tag{14}$$

$$\boldsymbol{n}\cdot\nabla^\star\delta\phi^\star = 0 \text{ on } \Omega_a \tag{15}$$

$$\boldsymbol{n}\cdot\nabla^* g_j^* = 0 \text{ on } \Omega_a,\ j = 1,2 \tag{16}$$

$$\boldsymbol{u}^\star = 0 \text{ on } \Omega_a \tag{17}$$

$$\boldsymbol{n}\cdot\nabla\phi_e^* = -\sigma_b^* \text{ on } \Omega_b \tag{18}$$

$$\boldsymbol{n}\cdot\nabla^\star\delta\phi^\star = 0 \text{ on } \Omega_b \tag{19}$$

$$\boldsymbol{n}\cdot\nabla^* g_j^* = 0 \text{ on } \Omega_b,\ j = 1,2 \tag{20}$$

$$\boldsymbol{u}^* = -\left(\frac{U}{U_{\mathrm{ref}}}\right)\boldsymbol{e}_z \text{ on } \Omega_b \tag{21}$$

$$\boldsymbol{n}\cdot\nabla\phi_e^* = -\sigma_c^* \text{ on } \Omega_c \tag{22}$$

$$\boldsymbol{n}\cdot\nabla^\star\delta\phi^\star = 0 \text{ on } \Omega_c \tag{23}$$

$$\boldsymbol{n}\cdot\nabla^* g_j^* = \frac{aU_{\mathrm{ref}}}{z_j D_j}(\boldsymbol{n}\cdot\boldsymbol{U}^*) \text{ on } \Omega_c,\ j = 1,2 \tag{24}$$

$$\boldsymbol{u}^* = -\left(\frac{U}{U_{\mathrm{ref}}}\right)\boldsymbol{e}_z \text{ on } \Omega_c \tag{25}$$

$$\boldsymbol{n}\cdot\nabla\phi_e^* = -\sigma_d^* \text{ on } \Omega_d \tag{26}$$

$$\boldsymbol{n}\cdot\nabla^\star\delta\phi^\star = 0 \text{ on } \Omega_d \tag{27}$$

$$\boldsymbol{n}\cdot\nabla^* g_j^* = \frac{aU_{\mathrm{ref}}}{z_j D_j}(\boldsymbol{n}\cdot\boldsymbol{U}^*) \text{ on } \Omega_d,\ j = 1,2 \tag{28}$$

$$\boldsymbol{u}^* = -\left(\frac{U}{U_{\mathrm{ref}}}\right)\boldsymbol{e}_z \text{ on } \Omega_d \tag{29}$$

$$\boldsymbol{n}\cdot\nabla\phi_e^* = -\sigma_n^* \text{ on } \Omega_n \tag{30}$$

$$\boldsymbol{n}\cdot\nabla^\star\delta\phi^\star = 0 \text{ on } \Omega_n \tag{31}$$

$$\boldsymbol{n}\cdot\nabla^* g_j^* = 0 \text{ on } \Omega_n,\ j = 1,2 \tag{32}$$

$$\boldsymbol{u}^* = -\left(\frac{U}{U_{\mathrm{ref}}}\right)\boldsymbol{e}_z \text{ on } \Omega_n \tag{33}$$

$\sigma_a^* = \sigma_a a/\varepsilon\zeta_a$, $\sigma_b^* = \sigma_b a/\varepsilon\zeta_a$, $\sigma_c^* = \sigma_c a/\varepsilon\zeta_a$, $\sigma_d^* = \sigma_d a/\varepsilon\zeta_a$, and $\sigma_n^* = \sigma_n a/\varepsilon\zeta_a$ are the scaled surface charge densities; $-U$ is the relative velocity of the pore; $\boldsymbol{n}$ and $\boldsymbol{e}_z$ are the unit outer normal vector directed into the fluid phase and the unit vector in the z direction, respectively.

We assume that both the fluid field and the electric field on Ω_i and Ω_o are independent of z, and the concentration of ionic species away from the particle is uninfluenced by its presence. These yield the following boundary conditions:

$$\boldsymbol{n}\cdot\nabla\phi_e^* = 0 \text{ on } \Omega_i \text{ and } \Omega_o \tag{34}$$

$$\boldsymbol{n}\cdot\nabla^\star\delta\phi^\star = -E^\star \text{ on } \Omega_i \text{ and } \Omega_o \tag{35}$$

$$g_j^* = -\delta\phi^* \text{ on } \Omega_i \text{ and } \Omega_o \tag{36}$$

$$\boldsymbol{n}\cdot\nabla u_z^* = 0 \text{ on } \Omega_i \text{ and } \Omega_o \tag{37}$$

$$u_r^* = 0 \text{ on } \Omega_i \text{ and } \Omega_o \tag{38}$$

Here, $E^\star = E/E_{\mathrm{ref}}$, $E_{\mathrm{ref}} = \zeta_a/k_B T$, $u_z^* = u_z/U_{\mathrm{ref}}$, and $u_r^* = u_r/U_{\mathrm{ref}}$; u_r and u_z are the r- and the z-components of the fluid velocity, respectively.

In addition, we assume that both the permittivity and the viscosity of the fluid phase inside the membrane layer are the same as that outside it, suggesting that the following quantities are continuous on Ω_m: ϕ_e^*, $\delta\phi^\star$, g_j^*, $\boldsymbol{n}\cdot\nabla\phi_e^*$, $\boldsymbol{n}\cdot\nabla^\star\delta\phi^\star$, $\boldsymbol{n}\cdot\nabla^* g_j^*$, $\boldsymbol{n}\cdot\boldsymbol{u}^\star$, $\boldsymbol{n}\times\boldsymbol{u}^\star$, $\boldsymbol{n}\cdot(\boldsymbol{\sigma}^{\boldsymbol{H}\star}\cdot\boldsymbol{n})$, and $\boldsymbol{n}\times(\boldsymbol{\sigma}^{\boldsymbol{H}\star}\cdot\boldsymbol{n})$.[20,36] Here, $\boldsymbol{\sigma}^{\boldsymbol{H}\star} = \boldsymbol{\sigma}^{\boldsymbol{H}}/[\varepsilon(\zeta_a)^2/a^2]$ is the scaled hydrodynamic stress tensor with $\boldsymbol{\sigma}^{\boldsymbol{H}} = -\delta p\boldsymbol{I} + 2\eta\Delta$ being the corresponding hydrodynamic stress tensor; $\boldsymbol{I}$, $\Delta = [\nabla\boldsymbol{u} + (\nabla\boldsymbol{u})^{\boldsymbol{T}}]/2$, and the superscript $\boldsymbol{T}$ are the unit tensor, the rate of deformation tensor, and matrix transpose, respectively. Note that using the present continuum model and the associated non-slip boundary condition is appropriate even when the EDL of the particle and that of the pore overlap.

This was demonstrated in the modeling of DNA electrophoresis in a nanopore, where a similar Poisson–Boltzmann (PB) type of continuum model was adopted, and non-slip boundary conditions assumed on the DNA and nanopore surfaces. This model was found to be capable of capturing the essential physics of the translocation of single dsDNA molecules through solid-state nanopores with radii larger than 5 nm,[53–55] where EDL overlapping can be significant.

Because the boundary conditions for the flow field contain the unknown particle velocity, the present problem needs to be solved by a trial-and-error procedure. This difficulty can be circumvented by partitioning it into two sub-problems.[10,20] In the first sub-problem, both the pore and the bulk fluid move at a constant relative velocity $-U$ in the absence of $\boldsymbol{E}$, and in the second sub-problem, $\boldsymbol{E}$ is applied, but both of them are stagnant. Let $\boldsymbol{F_k}$ and F_k be the total force acting on the particle in the z direction in sub-problem k and the corresponding magnitude, respectively. Then $F_1^* = \chi U^*$ and $F_2^* = \beta E^*$, where $F_k^* = F_k/\varepsilon(\zeta_a)^2$ are the scaled forces, and χ and β are proportionality constants. Because $F_1^* + F_2^* = 0$ at the steady state,

$$\mu^* = \frac{U^*}{E^*} = -\frac{F_2^*}{F_1^*}, \tag{39}$$

where μ^* and $U^* = U/U_{\mathrm{ref}}$ are the scaled electrophoretic mobility and the scaled velocity of the particle, respectively. In our case, $\boldsymbol{F_k}$ includes the electrical force $\boldsymbol{F_e}$ and hydrodynamic force $\boldsymbol{F_d}$. If we let F_{ek} and F_{dk} be the z components of $\boldsymbol{F_e}$ and $\boldsymbol{F_d}$ in sub-problem k, respectively, and $F_{ek}^* = \left(F_{ek}/\varepsilon(\zeta_a)^2\right)$ and $F_{dk}^* = \left(F_{dk}/\varepsilon(\zeta_a)^2\right)$ be the corresponding scaled quantities, then[20,48]

$$F_{ek}^* = \iint_{\Omega_m^*} \left(\varepsilon \frac{\partial \phi_e^*}{\partial n}\frac{\partial \delta\phi^*}{\partial z} - \varepsilon\left(\frac{\partial \phi_e^*}{\partial t}\frac{\partial \delta\phi^*}{\partial t}\right) n_z\right) \mathrm{d}\Omega_m^* \tag{40}$$

$$F_{dk}^* = \iint_{\Omega_m^*} (\boldsymbol{\sigma}^{\boldsymbol{H}^*} \cdot \boldsymbol{n}) \cdot \boldsymbol{e}_z \mathrm{d}\Omega_m^* \tag{41}$$

$\Omega_m^* = \Omega_m/a^2$ is the scaled surface area of the membrane layer, and $\boldsymbol{t}$ the unit tangential vector; $\partial/\partial n$ and $\partial/\partial t$ are the derivatives in the directions of these vectors, respectively; $\boldsymbol{n}_z$ is the z component of $\boldsymbol{n}$.

3. Results and discussion

3.1 Code verification

The present problem is solved numerically by FlexPDE (PDE Solutions, Spokane Valley, WA). To verify its applicability and the solution procedure adopted, the electrophoresis of a soft spherical particle composed of a rigid core of constant surface potential and an uncharged membrane layer in an infinite medium, which was solved analytically by Ohshima,[37] is solved. To simulate his conditions, we let $w = h = 0$ and $\sigma_b^* = \sigma_c^* = \sigma_d^* = \sigma_n^* = 0$, and b is assumed to be of a sufficiently large value (*e.g.*, $12a$). According to Hsu and Chen,[17] the end effect of the pore can be neglected if the pore length exceeds *ca.* 12 times of the particle radius. Fig. 2 shows the variation of the scaled mobility μ^* with λa; both the result of Ohshima and the corresponding result based on the present approach are illustrated. As can be seen in this figure, the performance of the software and the solution procedure is satisfactory. The slight deviation at small λa comes from the effect of double-layer polarization[13,20] and is neglected in Ohshima's study.

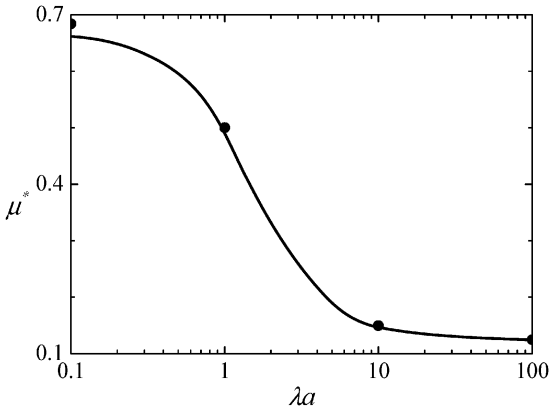

Fig. 2 Variation of the scaled mobility μ^* with λa for a soft spherical particle composed of a rigid core of constant surface potential and an uncharged membrane layer in an infinite liquid for the case where $\phi_e^* = 1$, $c/a = 1$, and $b/a = 12$. Solid curve: present result; discrete symbols: result of Ohshima.[37]

3.2 Numerical simulation

The electrophoretic behavior of a particle under various conditions is examined through a thorough numerical simulation by varying the thickness of the double layer (or bulk ionic concentration), the softness of the membrane layer of the particle, the shape of the pore, the distance between the particle and the throat center, and the charge density of the rigid surface of the particle and that of the pore. For illustration, we assume that the radius of the particle's rigid core is $a = 10$ nm, the thickness of its membrane layer, which is free of fixed charge (*i.e.*, $Q^* = 0$), is $c = 10$ nm, and the pore radius is $b = 5a$. To avoid the end effect of the pore, its length is assumed to have the value of $40a$. The liquid phase is an aqueous KCl solution, implying that $z_1 = -z_2$, $\alpha = 1$, and $\mathrm{Pe}_1 = \mathrm{Pe}_2 = 0.235$.[50]

3.3 Influence of λa

As can be seen in Fig. 3a, the particle mobility is influenced appreciably by the softness parameter λa: the larger its value the smaller the mobility, which has been observed in many studies.[41–43,56,57] This is because the larger the λa the greater the friction of the membrane layer of a particle. The scaled distance between the center of throat and that of the particle, (d/a), also plays an important role. Fig. 3a reveals that the smaller the $|d/a|$ the larger the mobility, implying that the particle mobility increases as it approaches the throat of the nanopore. In particular, μ^* has its maximum value at the center of the pore (*i.e.*, $d/a = 0$). This can be attributed to the enhanced local electric field due to the reduction in the cross sectional area of the nanopore.[29,58] A similar acceleration phenomenon of a particle as it approaches the necked area of a pore was observed experimentally in the electrokinetic[31] and

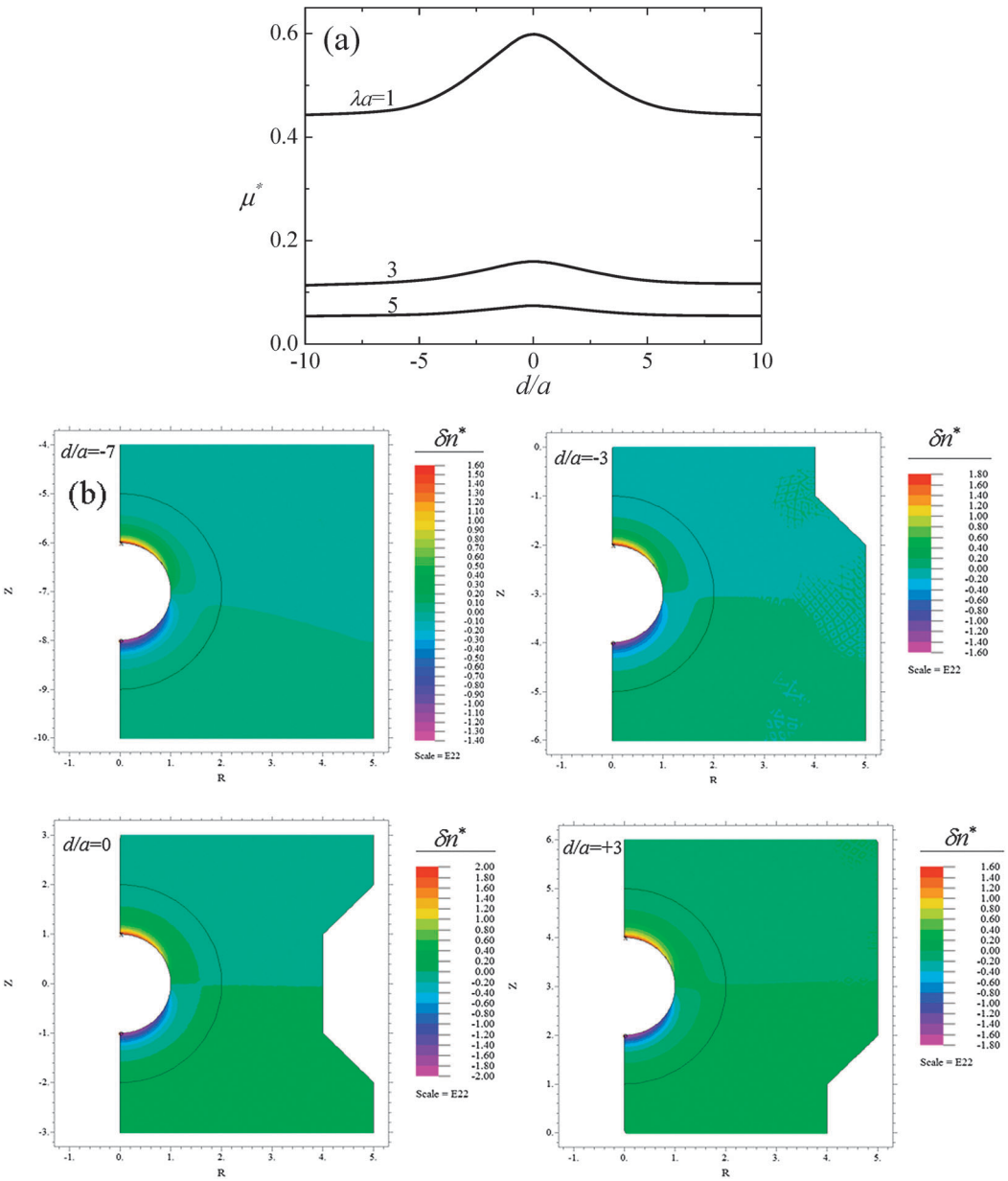

Fig. 3 (a) Variations of the scaled mobility μ^* as a function of (d/a) for various values of λa at $\sigma_a^* = 4$, $\sigma_n^* = 0$, $\kappa a = 3$, $w/a = h/a = 1$, and $l/a = 2$. (b) Contours of the scaled perturbed ion distribution $\delta n^* = [(n_2 - n_{2e}) - (n_1 - n_{1e})]/n_{10}$ for various values of (d/a) on the plane $\theta = \pi/2$ at $\sigma_a^* = 4$, $\sigma_n^* = 0$, $\kappa a = 3$, $\lambda a = 3$, $w/a = h/a = 1$, and $l/a = 2$.

pressure-driven[28] transport of particles through a converging–diverging microchannel.

To further examine the influence of the particle position in the necked area of the nanopore on the local electric field, we plot the spatial variations of the scaled perturbed ion distribution, $\delta n^* = [(n_2 - n_{2e}) - (n_1 - n_{1e})]/n_{10}$, for various values of (d/a) in Fig. 3b. Note that the strength of the electric field is proportional to $|\delta n^*|$. Note that the strongest electric field occurs at $d/a = 0$, yielding the maximum μ^* seen in Fig. 3a. However, the larger the λa the less significant the acceleration of the particle due to the decrease in $|d/a|$. This is because as λa gets large, the hydrodynamic drag coming from the particle's membrane layer becomes significant, thereby reducing the influence of the enhanced local electric field on the particle mobility in the throat region of the nanopore. We conclude that the presence of the throat is capable of influencing both the flow and the electric fields, thereby enhancing the particle mobility.

3.4 Influences of σ_a^* and κa

The influences of the charge density on the particle's rigid core surface, measured by σ_a^*, and the thickness of the double layer, measured by κa, are summarized in Fig. 4. Fig. 4a indicates that the smaller the σ_a^* the smaller the μ^* and the less appreciable the presence of the maximum of μ^*. This is expected because the smaller the σ_a^* the smaller the electric driving force acting on

the particle. It is interesting to see in Fig. 4b that the behavior of μ^* as κa varies depends upon the level of σ_a^*. If σ_a^* is small (*e.g.*, 2), μ^* deceases with the increasing κa in the range of 0.2 to 1; however, if it is sufficiently large (*e.g.*, 6), μ^* shows a local maximum as κa varies.

The former can be explained by the reduction in the effective charge density due to the increase in κa.[49,59] If κa is small (thick EDL), the membrane layer of the particle is totally enclosed by EDL, and counterions stay mainly outside EDL. On the other hand, if κa is sufficiently large (thin EDL), because the counterion concentration inside the membrane layer becomes appreciable, its effective charge, $|\rho + \rho_{fix}|$, decreases accordingly. Therefore, $\mu^*(\kappa a = 0.2) > \mu^*(\kappa a = 0.5) > \mu^*(\kappa a = 1)$. This behavior was also observed by Yeh *et al.*[42] in a study of the electrophoresis of a soft biocolloid in a spherical cavity. If σ_a^* is large, $\mu^*(\kappa a = 0.5) > \mu^*(\kappa a = 0.2) > \mu^*(\kappa a = 1)$. This arises from the intensification of the local electric field near the particle.[50] Because this effect becomes most significant if the particle's charge density is high and the thickness of EDL is thick, μ^* increases with increasing κa for smaller κa, and decreases with increasing κa for larger κa. To further understand the effects of the EDL thickness and the surface charge density of a soft particle as it locates within the necked area of the pore, we plot the particle mobility at $d/a = 0$ *versus* κa for various values of σ_a^* in Fig. 4c. As expected, μ^* shows a local maximum as κa varies. Fig. 4c also reveals that the critical value of κa at which μ^* has the local maximum increases with increasing σ_a^*. Since the intensification of the local electric field near the particle is significant if σ_a^* is large,[50] the behavior that μ^* increases with increasing κa at small κa becomes appreciable.

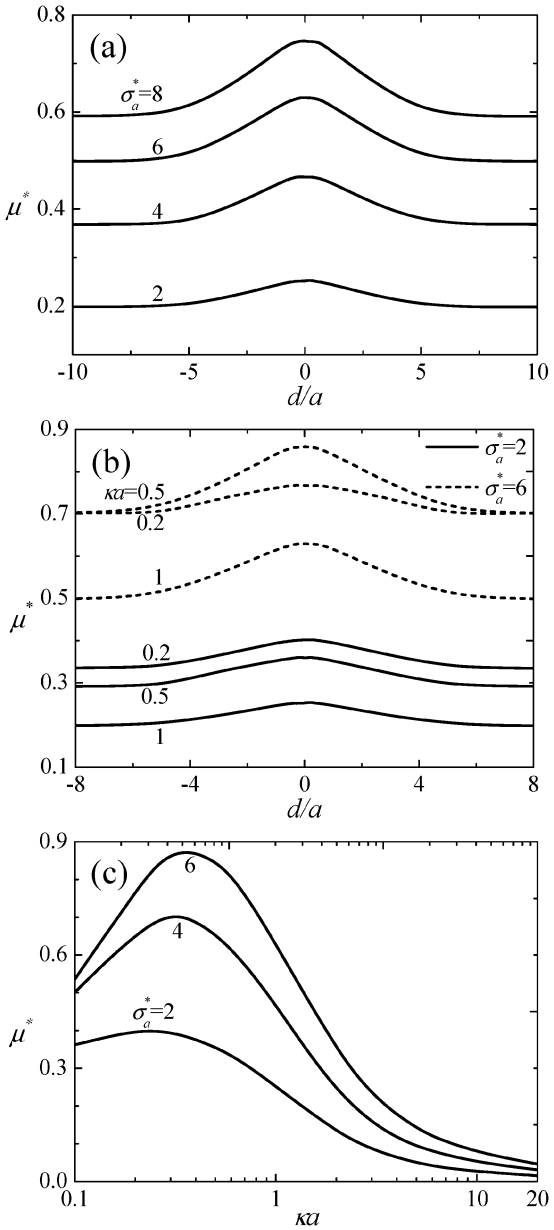

Fig. 4 Variations of the scaled mobility μ^* as a function of (d/a) for various values of σ_a^* at $\sigma_n^* = 0$, $\kappa a = 3$, $\lambda a = 3$, $w/a = h/a = 1$, and $l/a = 2$, (a), and for various combinations of κa and σ_a^* at $\sigma_n^* = 0$, $\lambda a = 3$, $w/a = h/a = 1$, and $l/a = 2$, (b). Variations of μ^* as a function of κa for various values of σ_a^* for the case of (b) at $d/a = 0$, (c). Solid curve in (b), $\sigma_a^* = 2$; dash curve, $\sigma_a^* = 6$.

3.5 Influence of (l/a)

The influence of the throat length, measured by (l/a), on the mobility of a particle is summarized in Fig. 5. As (l/a) increases, so does the length of the throat region, and therefore, the nearby local electric field intensifies accordingly, which was also observed previously.[29,30] This implies that the increase of μ^* due to the presence of the throat section is enhanced. As expected, the influence of (l/a) on μ^* becomes negligible as the particle is far from the throat. The slight disturbance of $\mu^*(l/a = 0)$ at $d/a \cong 0$ arises from a strong interaction between the double layer and the nanopore surface.

3.6 Influence of σ_n^*

Fig. 6 shows the influence of the pore charge density, measured by σ_n^*, on the mobility of a particle. For illustration, we assume that the throat section of the pore is positively charged, implying that the electroosmotic flow (EOF) induced is in the direction opposite to that of the applied electric field.

Fig. 6 shows that the qualitative behavior of the particle mobility is uninfluenced by σ_n^*. This arises from the fact that

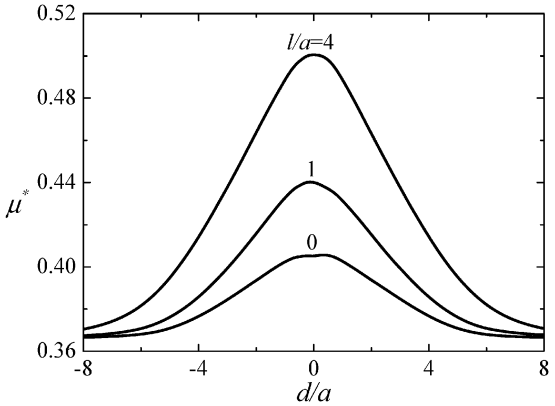

Fig. 5 Variations of the scaled mobility μ^* as a function of (d/a) for various values of (l/a) at $\sigma_a^* = 4$, $\sigma_n^* = 0$, $\kappa a = 1$, $\lambda a = 3$, and $w/a = h/a = 1$.

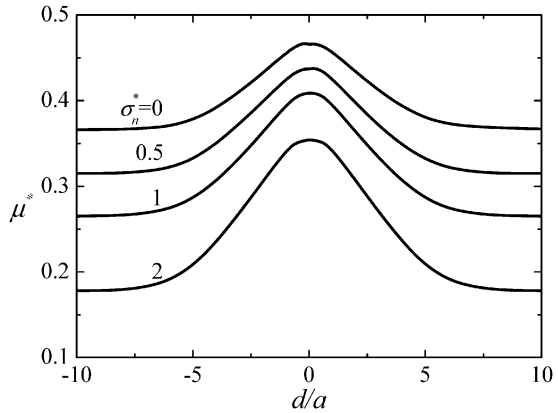

Fig. 6 Variations of the scaled mobility μ^* as a function of (d/a) for various values of σ_n^* at $\sigma_a^* = 4$, $\kappa a = 1$, $\lambda a = 3$, $w/a = h/a = 1$, and $l/a = 2$.

although the particle mobility would be retarded by the EOF due to a positive σ_n^*, the local electric field acting on the particle is simultaneously intensified and becomes dominant as it translates in the necked area of a pore, resulting in a greater electrical driving force. Fig. 6 also reveals that as σ_n^* increases, so does the strength of the induced EOF, μ^* decreases accordingly, implying that the accelerated–decelerated behavior of the particle as it locates within the necked area of the pore is not influenced by the EOF. Since the EOF at $\sigma_n^* = 2$ is stronger than those at other smaller values of σ_n^*, the corresponding μ^* becomes the smallest. However, it is interesting to see that the ratio of $[\mu^*(d/a = 0)/\mu^*(d/a \to \infty)]$ at $\sigma_n^* = 2$ is larger than those at other values of σ_n^*. This implies that raising the charge density of the throat section is capable of raising the efficiency of particle acceleration, and therefore, the separation efficiency.

4. Conclusions

The influence of boundary shape on electrophoresis is modeled by considering a soft spherical particle comprising a positively charged rigid core and an uncharged membrane layer on the axis of a necked cylindrical pore with its throat positively charged. We show that the presence of the throat makes the associated flow and electric fields nonuniform, yielding interesting electrophoretic behaviors. The results of numerical simulation can be summarized as follows. (i) The reduction in the cross-section area of the pore intensifies the local electric field, and therefore, accelerates the particle. Raising the softness parameter of the membrane layer makes this effect less important. (ii) The reduction in the cross-section area of the pore also makes the ionic distribution nonuniform, and the electric field induced accelerates the particle. (iii) The mobility of the particle increases with increasing charge density on its rigid core. (iv) If the particle charge density is low, the mobility decreases with decreasing double layer thickness, which is due to the counterion condensation inside the membrane layer. On the other hand, if it is high, the competition between the local electric field and the effective charge density of the particle yields a local maximum in the mobility as the double layer thickness varies. (v) Due to that the local electric field is intensified, the mobility increases with the throat length. However, because the throat is positively charged, the associated electroosmotic flow reduces the mobility. (vi) The maximum mobility occurs at the center of a throat, and the higher the charge density of the throat the larger the ratio of maximum mobility/mobility far away from the throat.

Acknowledgements

This work is supported by the National Science Council of the Republic of China.

Notes and references

1 T. M. Squires and S. R. Quake, *Rev. Mod. Phys.*, 2005, **77**, 977–1026.
2 Y. J. Kang and D. Q. Li, *Microfluid. Nanofluid.*, 2009, **6**, 431–460.
3 X. C. Xuan, J. J. Zhu and C. Church, *Microfluid. Nanofluid.*, 2010, **9**, 1–16.
4 S. Patel, D. Showers, P. Vedantam, T. R. Tzeng, S. Z. Qian and X. C. Xuan, *Biomicrofluidics*, 2012, **6**, 034102.
5 S. Howorka and Z. Siwy, *Chem. Soc. Rev.*, 2009, **38**, 2360–2384.
6 B. M. Venkatesan and R. Bashir, *Nat. Nanotechnol.*, 2011, **6**, 615–624.
7 W. J. Lan, D. A. Holden, B. Zhang and H. S. White, *Anal. Chem.*, 2011, **83**, 3840–3847.
8 R. Vogel, W. Anderson, J. Eldridge, B. Glossop and G. Willmott, *Anal. Chem.*, 2012, **84**, 3125–3131.
9 N. Hu, Y. Ai and S. Z. Qian, *Sens. Actuators, B*, 2012, **161**, 1150–1167.
10 R. W. O'brien and L. R. White, *J. Chem. Soc., Faraday Trans. 2*, 1978, **74**, 1607–1626.
11 E. Yariv, *Phys. Fluids*, 2005, **17**, 051702.
12 J. P. Hsu and Y. H. Tai, *Langmuir*, 2010, **26**, 16857–16864.
13 L. H. Yeh, K. L. Liu and J. P. Hsu, *J. Phys. Chem. C*, 2012, **116**, 367–373.
14 S. Bhattacharyya and P. P. Gopmandal, *Soft Matter*, 2013, **9**, 1871–1884.
15 H. J. Keh and J. L. Anderson, *J. Fluid Mech.*, 1985, **153**, 417–439.
16 H. Liu, H. H. Bau and H. H. Hu, *Langmuir*, 2004, **20**, 2628–2639.
17 J. P. Hsu and Z. S. Chen, *Langmuir*, 2007, **23**, 6198–6204.
18 S. Z. Qian, S. W. Joo, W. S. Hou and X. X. Zhao, *Langmuir*, 2008, **24**, 5332–5340.
19 S. W. Joo and S. Z. Qian, *J. Colloid Interface Sci.*, 2011, **356**, 331–340.
20 L. H. Yeh and J. P. Hsu, *Soft Matter*, 2011, **7**, 396–411.
21 C. H. Huang and E. Lee, *J. Phys. Chem. C*, 2012, **116**, 15058–15067.
22 C. H. Huang, H. P. Hsu and E. Lee, *Phys. Chem. Chem. Phys.*, 2012, **14**, 657–667.

23 Y. Ai and S. Z. Qian, *Phys. Chem. Chem. Phys.*, 2011, **13**, 4060–4071.
24 M. L. Plenert and J. B. Shear, *Proc. Natl. Acad. Sci. U. S. A.*, 2003, **100**, 3853–3857.
25 D. Kozak, W. Anderson, R. Vogel, S. Chen, F. Antaw and M. Trau, *ACS Nano*, 2012, **6**, 6990–6997.
26 Y. J. Kang, D. Q. Li, S. A. Kalams and J. E. Eid, *Biomed. Microdevices*, 2008, **10**, 243–249.
27 J. J. Zhu, G. Q. Hu and X. C. Xuan, *Electrophoresis*, 2012, **33**, 916–922.
28 Y. Ai, S. W. Joo, Y. T. Jiang, X. C. Xuan and S. Z. Qian, *Biomicrofluidics*, 2009, **3**, 022404.
29 S. Z. Qian, A. H. Wang and J. K. Afonien, *J. Colloid Interface Sci.*, 2006, **303**, 579–592.
30 Y. Ai, S. W. Joo, Y. T. Jiang, X. C. Xuan and S. Z. Qian, *Electrophoresis*, 2009, **30**, 2499–2506.
31 X. C. Xuan, B. Xu and D. Q. Li, *Anal. Chem.*, 2005, **77**, 4323–4328.
32 Y. Ai, S. Z. Qian, S. Liu and S. W. Joo, *Biomicrofluidics*, 2010, **4**, 013201.
33 J. B. Heng, A. Aksimentiev, C. Ho, P. Marks, Y. V. Grinkova, S. Sligar, K. Schulten and G. Timp, *Nano Lett.*, 2005, **5**, 1883–1888.
34 A. G. Balducci, J. Tang and P. S. Doyle, *Macromolecules*, 2008, **41**, 9914–9918.
35 Q. J. Chen, S. Diao and C. Wu, *Soft Matter*, 2012, **8**, 5451–5458.
36 H. Ohshima, *Adv. Colloid Interface Sci.*, 1995, **62**, 189–235.
37 H. Ohshima, *J. Colloid Interface Sci.*, 2002, **252**, 119–125.
38 J. F. L. Duval and H. Ohshima, *Langmuir*, 2006, **22**, 3533–3546.
39 R. J. Hill, D. A. Saville and W. B. Russel, *J. Colloid Interface Sci.*, 2003, **258**, 56–74.
40 L. H. Yeh, M. K. Zhang, S. W. Joo, S. Qian and J. P. Hsu, *Anal. Chem.*, 2012, **84**, 9615–9622.
41 C. H. Huang, W. L. Cheng, Y. Y. He and E. Lee, *J. Phys. Chem. B*, 2010, **114**, 10114–10125.
42 L. H. Yeh, K. Y. Fang, J. P. Hsu and S. Tseng, *Colloids Surf., B*, 2011, **88**, 559–567.
43 M. K. Zhang, Y. Ai, D. S. Kim, J. H. Jeong, S. W. Joo and S. Z. Qian, *Colloids Surf., B*, 2011, **88**, 165–174.
44 M. K. Zhang, L. H. Yeh, S. Z. Qian, J. P. Hsu and S. W. Joo, *J. Phys. Chem. C*, 2012, **116**, 4793–4801.
45 R. B. Schoch, J. Y. Han and P. Renaud, *Rev. Mod. Phys.*, 2008, **80**, 839–883.
46 L. H. Yeh, M. Zhang, S. Qian, J. P. Hsu and S. Tseng, *J. Phys. Chem. C*, 2012, **116**, 8672–8677.
47 L. H. Yeh, M. Zhang, N. Hu, S. W. Joo, S. Qian and J. P. Hsu, *Nanoscale*, 2012, **4**, 5169–5177.
48 J. P. Hsu, L. H. Yeh and M. H. Ku, *J. Colloid Interface Sci.*, 2007, **305**, 324–329.
49 L. H. Yeh, Y. H. Tai, N. Wang, J. P. Hsu and S. Z. Qian, *Nanoscale*, 2012, **4**, 7575–7584.
50 J. P. Hsu, H. M. Lo, L. H. Yeh and S. Tseng, *J. Phys. Chem. B*, 2012, **116**, 12626–12632.
51 J. F. L. Duval and F. Gaboriaud, *Curr. Opin. Colloid Interface Sci.*, 2010, **15**, 184–195.
52 M. Zembala, *Adv. Colloid Interface Sci.*, 2004, **112**, 59–92.
53 S. Ghosal, *Phys. Rev. Lett.*, 2007, **98**, 238104.
54 S. van Dorp, U. F. Keyser, N. H. Dekker, C. Dekker and S. G. Lemay, *Nat. Phys.*, 2009, **5**, 347–351.
55 Y. H. He, M. Tsutsui, C. Fan, M. Taniguchi and T. Kawai, *ACS Nano*, 2011, **5**, 5509–5518.
56 H. Ohshima, *Electrophoresis*, 2006, **27**, 526–533.
57 H. J. Keh and C. P. Liu, *J. Phys. Chem. C*, 2010, **114**, 22044–22054.
58 L. H. Yeh, M. K. Zhang, S. Z. Qian and J. P. Hsu, *Nanoscale*, 2012, **4**, 2685–2693.
59 L. H. Yeh, J. P. Hsu, S. Qian and S. J. Tseng, *Electrochem. Commun.*, 2012, **19**, 97–100.